Analytical Biochemistry 394 (2009) 39–47

Contents lists available at ScienceDirect

Analytical Biochemistry

journal homepage: www.elsevier.com/locate/yabio

A homogeneous resonance energy transfer assay for phosphopantetheinyl transferase

Timothy L. Foley, Michael D. Burkart *

Department of Chemistry and Biochemistry, University of California, San Diego, La Jolla, CA 92093, USA

ARTICLE INFO

Article history:
Received 10 April 2009
Available online 30 June 2009

Keywords:
Phosphopantetheinyl transferase
Assay development
High-throughput screen
FRET assay
Fluorescent analogue
Coenzyme A
Acyl carrier protein
Peptidyl carrier protein
Secondary metabolism

ABSTRACT

Phosphopantetheinyl transferase plays an essential role in activating fatty acid, polyketide, and nonribosomal peptide biosynthetic pathways, catalyzing covalent attachment of a 4′-phosphopantetheinyl group to a conserved residue within carrier protein domains. This enzyme has been validated as an essential gene to primary metabolism and presents a target for the identification of antibiotics with a new mode of action. Here we report the development of a homogeneous resonance energy transfer assay using fluorescent coenzyme A derivatives and a surrogate peptide substrate that can serve to identify inhibitors of this enzyme class. This assay lays a blueprint for translation of these techniques to other transferase enzymes that accept fluorescent substrate analogues.

Published by Elsevier Inc.

A unifying characteristic in the biosynthesis of fatty acid, nonribosomal peptide, and polyketide compounds is the tethering of the nascent polymer to small carrier protein domains of the synthases through thioester linkage about a 4′-phosphopantetheinyl (4′-PP)[1] arm. This 4′-PP is installed on the proteins posttranslationally from coenzyme A (CoA) **2** on a conserved serine residue by action of phosphopantetheinyl transferase (PPTase) enzymes, converting them from their *apo*-**1** to *holo*-**4** forms (Fig. 1). This modification is essential for synthase activity, and ablation of the PPTase gene precludes natural product production [1–4] or, in the case of fatty acid biosynthesis, renders the organism unviable [3–5]. Within bacteria, there exist two major enzyme classes of the PPTase superfamily: the AcpS type and the Sfp type [1]. Groupings in these designations are made based on primary sequence, and their canonical representatives, AcpS of *Escherichia coli* and Sfp of *Bacillus subtilis*, are structurally distinct [6,7].

It has been demonstrated that *acpS* is an essential *E. coli* gene [8,9], thereby validating it as a target for inhibitor development with the potential to treat multidrug resistance. Indeed, a number of groups have begun focused programs to develop AcpS inhibitors [10–14], and several candidates have been discussed recently [10–12]. In addition to fatty acids, a number of compounds are produced from 4′-PP-dependent pathways that have been identified as virulence factors, and disruption of their biosynthesis has received much attention as a new angle for therapeutic development [15–19]. We have been intrigued by the central role of phosphopantetheinylation in these metabolic pathways and are interested in studying the potential effects that PPTase inhibitors may have on the coordinate attenuation of numerous aspects of pathogenicity.

Although AcpS-directed inhibitor development has been reported [10–14], this work has generally omitted screening protocols. The only described method uses homogeneous time-resolved fluorescence resonance energy transfer (FRET) as a means for activity determination [11]. We found replication of this technique to be beyond our capabilities due to limitations imposed by instrumentation, and we desired the use of readily available and affordable biochemical reagents. Here we report the development of a homogeneous FRET screen for the two canonical PPTase representatives: AcpS and Sfp. This method is simple, requiring only the addition of reagents to reaction wells of a microtiter plate, and here we validate it as a process to identify inhibitors of these enzymes. Furthermore,

* Corresponding author. Fax: +1 858 882 1174.
E-mail address: mburkart@ucsd.edu (M.D. Burkart).

[1] *Abbreviations used:* 4′-PP, phosphopantetheinyl; CoA, coenzyme A; PPTase, phosphopantetheinyl transferase; FRET, fluorescence resonance energy transfer; DACM, 7-dimethylamino-4-methyl-coumarin-3-maleimide; TAMRA, *N,N,N′,N′*-tetramethylrhodamine-5-maleimide; PAP, 3′-phosphoadenosine-5′-phosphate; Hepes, 4-(2-hydroxyethyl)-1-piperazine ethanesulfonic acid; DMSO, dimethyl sulfoxide; FITC, fluorescein-5-isothiocyanate; UV–Vis, ultraviolet–visible; BSA, bovine serum albumin; Fmoc, 9-fluorenylmethyloxycarbonyl; HATU, 2-(1H-7-azabenzotriazol-1-yl)-1,1,3,3-tetramethyl uronium hexafluorophosphate; HPLC, high-performance liquid chromatography; ESI–MS, electrospray ionization–mass spectrometry; mCoA, fluorescence reporter-modified coenzyme A; ACP, acyl carrier protein; SPPS, solid phase peptide synthesis; RFU, relative fluorescence units.

0003-2697/$ - see front matter Published by Elsevier Inc.
doi:10.1016/j.ab.2009.06.037

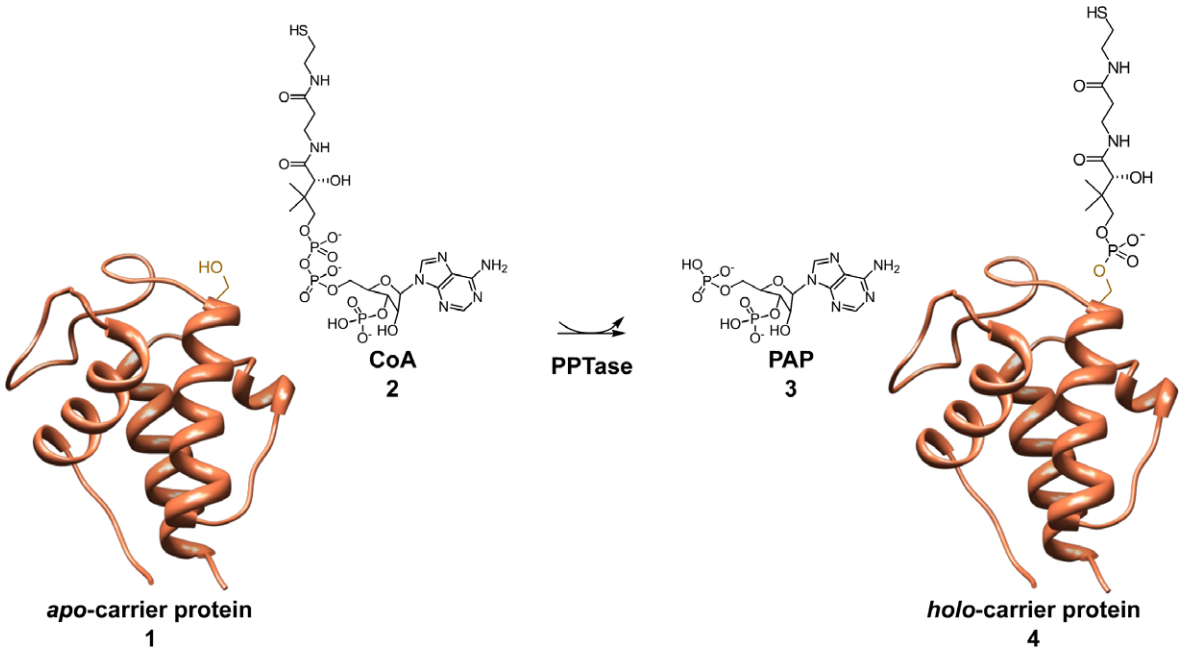

Fig. 1. Posttranslational modification of carrier proteins. The translated *apo*-carrier proteins **1** and coenzyme A **2** react with PPTase to generate 3′-phosphoadenosine-5′-phosphate (PAP) **3** and *holo*-carrier proteins **4**.

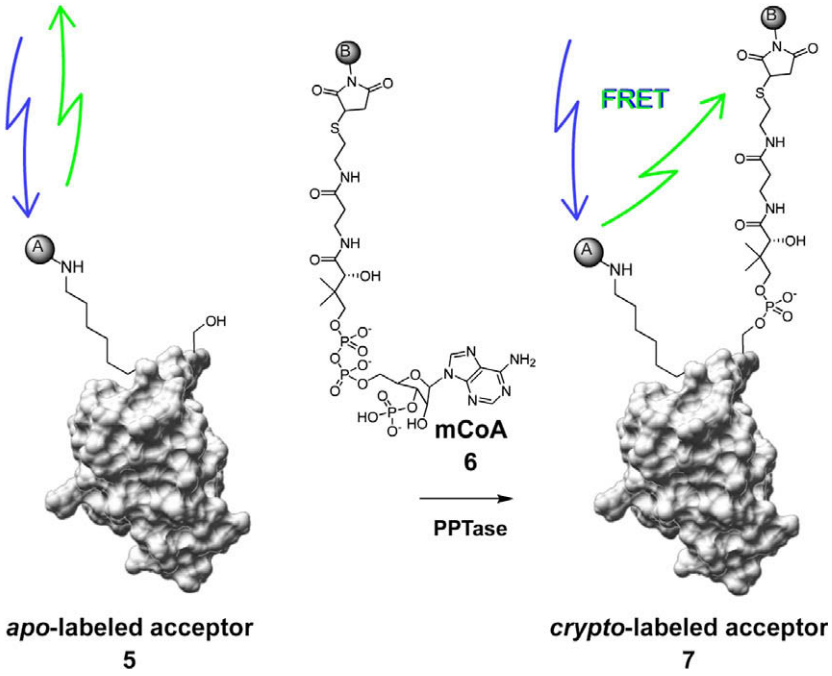

Fig. 2. FRET assay for PPTase. Action of PPTase on a fluorescently labeled acceptor substrate **5**, in conjunction with mCoA **6**, assembles a FRET pair on conversion to the thiol-blocked *crypto*-acceptor substrate **7**. The assembly of this FRET pair can be detected with a fluorescence microplate reader.

we describe the details that led to successful development of this screen so that it may serve to blueprint assay design for other transferase enzymes that accept reporter-modified substrate analogues.

Materials and methods

General

7-Dimethylamino-4-methyl-coumarin-3-maleimide (DACM) and *N*,*N*,*N*′,*N*′-tetramethylrhodamine-5-maleimide (TAMRA) were purchased from Invitrogen (Carlsbad, CA, USA). CoA trilithium salt was purchased from EMD Biochemicals (San Diego, CA, USA). 3′-Phosphoadenosine-5′-phosphate disodium salt (PAP), 4-(2-hydroxyethyl)-1-piperazine ethanesulfonic acid (Hepes), dimethyl sulfoxide (DMSO, Hybri-Max grade), and fluorescein-5-isothiocyanate isomer I (FITC) were purchased from Sigma (St. Louis, MO, USA). Concentrations of all fluorescently labeled reagents were quantified by ultraviolet–visible (UV–Vis) spectroscopy with an Agilent 8354 diode array spectrophotometer (Agilent Technologies, Santa Clara, CA, USA) using the following extinction coefficients: DACM, 23,000 cm^{-1} M^{-1}; FITC, 77,000 cm^{-1} M^{-1}; TAMRA, 95,000 cm^{-1} M^{-1}.

Enzyme expression and purification

Sfp was expressed and purified as described previously [2]. The enzyme was concentrated to 40 mg/ml, diluted with an equal volume of 75% glycerol, and stored in 100-μl aliquots at −80 °C. For routine use, this stock (20 mg/ml, 765 μM) was diluted to 1 mg/ml in Sfp storage buffer (50 mM Na–Hepes, 120 mM NaCl, and 33% [v/v] glycerol) supplemented with 0.1% (w/v) bovine serum albumin (BSA) and stored at −20 °C. Under these conditions, there was no noticeable reduction in enzymatic activity with storage for periods longer than 6 months.

Escherichia coli AcpS was expressed and purified as a native protein from pDPJ according to published procedures [20]. The protein concentration of the final preparation was adjusted to 10 mg/ml by the addition of 2× storage buffer, an equal volume of glycerol added in three portions, and aliquots stored at −80 °C. For routine work, single tubes (200-μl portions) were stored at −20 °C, with no degradation of enzymatic activity observed after 1 year of storage.

Synthesis of assay components

An exploratory quantity (~8 mg) of FITC-modified YbbR peptide (FITC–YbbR) **8** (sequence: fluorescein-Ahx-DSLEFIASKLA-OH) was initially purchased from GL Biochem (Shanghai, China). For the final screen evaluation, the peptide was prepared on the 0.2-mmol scale using an automated solid phase peptide synthesizer (Pioneer, Applied Biosystems, Foster City, CA, USA) using standard 9-fluorenylmethyloxycarbonyl (Fmoc) chemistry with 2-(1H-7-azabenzotriazol-1-yl)-1,1,3,3-tetramethyl uronium hexafluorophosphate (HATU) activation (see Fig. 3A) [21]. The sequence was appended with an N-terminal *N*-Fmoc–ε-aminocaproic acid spacer, deprotected, and coupled overnight with FITC. Following cleavage from the solid support, the product was high-performance liquid chromatography (HPLC) purified to yield 84 mg of FITC–YbbR **8,** and its identity was verified by electrospray ionization–mass spectrometry (ESI–MS).

Fluorescence reporter-modified CoA (mCoA) analogues **11** and **12** were prepared by reaction of reduced CoA trilithium salt **2** (1 mg/ml in 50 mM NaH_2PO_4, pH 7.4) with 1.1 equivalents of maleimide-bearing probes **9** and **10**, respectively (both dissolved at 1 mg/ml in methanol) (see Fig. 3B). The reaction was followed to completion by HPLC, determined by disappearance of the CoA peak. Excess **9** and **10** was removed by extraction three times with ethyl acetate and dichloromethane, respectively. The resultant aqueous phase was placed under vacuum (<2 mm/Hg) for 2 h to remove residual organic solvent. The purity of mCoA analogues **11** and **12** was verified to be greater than 95% by HPLC.

Kinetic evaluation of fluorescent substrates

Kinetic parameters for FITC–YbbR **8** and TAMRA–mCoA **12** were determined by HPLC. Reactions were conducted in a final volume of 50 μl in a buffer containing 10 mM $MgCl_2$, 50 mM Na–Hepes (pH 7.6), and 0.1 mg/ml BSA. Reactions were initiated by the addition of 0.5 μM enzyme, allowed to progress for 15 min, and quenched by the addition of 50 μl of 50 mM sodium ethylenediaminetetraacetic acid (pH 8.0). The reaction mixtures were then separated by reversed phase chromatography with an Agilent 1100 instrument fitted with a diode array detector (Agilent Technologies) using an OD5 C_{18} column (250 × 4.6 mm, Cat. No. 9575, Burdick & Jackson, Morristown, NJ, USA). The separation was performed under the following conditions: buffer A, 10 mM ammonium acetate; buffer B, acetonitrile; flow rate, 1.5 ml/min. After injection, the run initiated with a 2-min isocratic flow of 10% buffer B, followed by sample elution with a 10-min linear gradient from 10% to 60% buffer B. The column was regenerated with a 2-min isocratic flow of 100% buffer B, and then the column equilibrated to 10% buffer B.

Fluorescence spectroscopy

Steady-state single sample fluorescence spectra were recorded on a QuantaMaster 2000 spectrofluorometer (Photon Technologies International, Princeton, NJ, USA) using excitation and emission slit widths of 4 nm and integration times of 0.1 s.

FRET screen conditions

PAP parent inhibitor plates were made by dissolving the compound in dry DMSO at a concentration of 10 mM and serial diluting

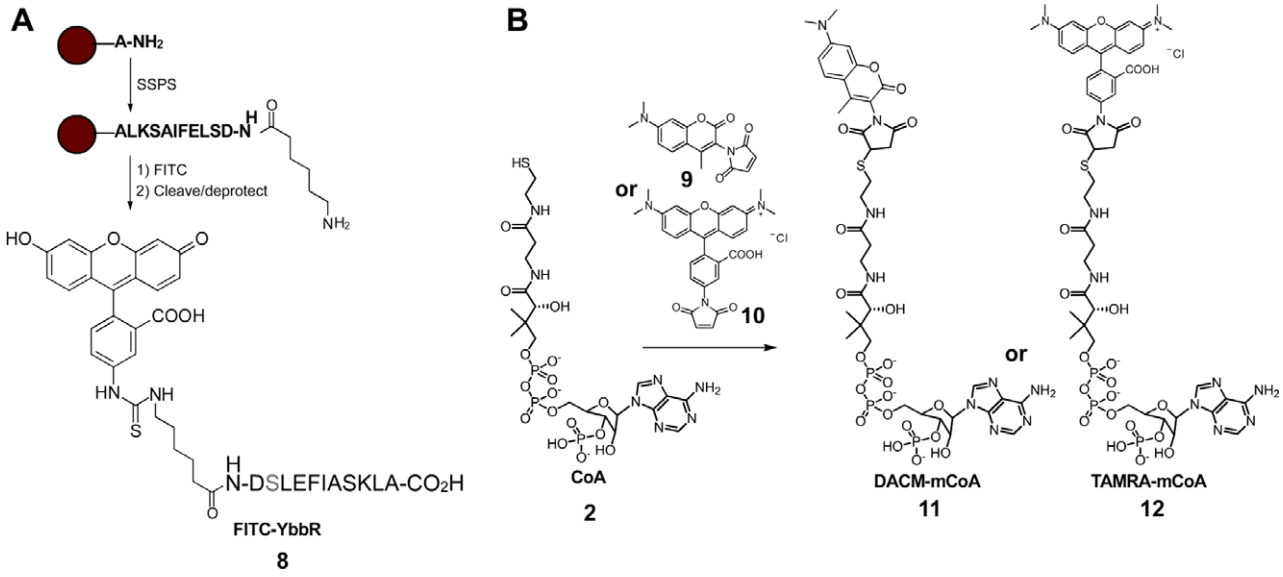

Fig. 3. Synthesis of assay components. (A) Beginning with L-alanine-loaded polystyrene resin, standard SPPS procedures afford the YbbR sequence appended with an ε-aminocaproic acid residue. Reaction with FITC, followed by cleavage and HPLC purification, gives the FITC–YbbR peptide substrate **8**. (B) CoA **2** is reacted with maleimide-bearing probes **9** and **10** to produce their fluorescent mCoA derivatives **11** and **12**, respectively.

this (twofold) in DMSO. The final protocol (Table 1) is as follows. First, 2.5 μl of the parent DMSO solutions (or DMSO as a negative control) was transferred to individual wells of a black polystyrene 96-well plate (Costar 3694), followed by 37.5 μl of a 1.33× enzyme solution (16.62 nM Sfp or 66.6 nM AcpS) in 1.33× PPTase assay buffer (66 mM Na–Hepes, 13.3 mM $MgCl_2$, and 1.33 mg/ml BSA, pH 7.6). Reactions were initiated by the addition of 10 μl of 5× reagent solution (50 μM TAMRA–mCoA **12**, 25 μM FITC–YbbR **8**, and 10 mM NaH_2PO_4, pH 7.0). The reaction was monitored continuously (cycle time 2 min) for 15 cycles in a PerkinElmer HTS 7000 Plus microtiter plate reader with excitation filter λ = 485 nm and emission filter λ = 535 nm.

Data analysis

Kinetic data were processed with Microsoft Excel. Assay statistics were evaluated according to standard equations [22]. Plotting and nonlinear regression were performed with GraphPad Prism (version 5.00, GraphPad Software, San Diego, CA, USA), and IC_{50} curves were fit with the four-parameter dose–response equation using the ordinary (least squares) setting. In all cases, error bars and reported error values represent 1 standard deviation.

Molecular graphics images (Figs. 1 and 2) are renditions of the *apo*-actinorhodin acyl carrier protein (PDB identifier: 2K0Y) and were generated using the UCSF Chimera package [23].

Results and discussion

Design of a high-throughput PPTase assay

Traditionally, PPTase bioassays have been conducted in a low-throughput manner either by monitoring radiolabel incorporation to precipitated protein mass from [^{3}H]-CoA [4] or by HPLC separation of the *apo*- and *holo*- states of the carrier protein substrate [3]. These systems use centrifugation and chromatographic separations, respectively, and are not readily amenable to high-throughput screening. In designing a high-throughput screen for PPTase activity, we desired a system that would allow direct monitoring of reaction progress to eliminate the probability of false-positive hits that arrive from inhibition of coupled enzyme systems. To accomplish this, we chose to exploit the synthetic aspect of the PPTase reaction in conjunction with an mCoA technology developed previously in our laboratory [24]. In this system, fluorophore-appended carrier protein domains/mimics **5** generate a FRET signal on conversion to their thiol-blocked *crypto*- form **7** by modification with mCoA **6** analogues by PPTase (Fig. 2).

Fluorescent probe selection and substrate synthesis

We chose to make an FITC modification to the protein-based substrate because this fluorophore possesses absorption and emission centered about the visible light spectrum, allowing it to function as either FRET donor or acceptor, depending on the identity of compounds chosen for mCoA **6** preparation (Fig. 2). This would allow us to probe both modes of FRET from a singly prepared pool of reagent. In turning to select a carrier protein domain to function as the acceptor substrate, we initially considered the *E. coli* fatty acid synthase acyl carrier protein (ACP) as a candidate because previous reports noted that ACP contains a single tyrosine residue present at the C terminus of α-helix 3 and modification of this residue with a dansyl moiety does not hinder its function [25,26]. We found this protocol and other tyrosine-modifying techniques [27,28] to provide low yields of fluorescein-modified proteins due to the insolubility of FITC and its derivatives in low pH reaction conditions (data not shown), and the purification of this labeled material was insufficient for our needs.

Subsequently, we chose to investigate the use of the 11-residue YbbR peptide (sequence: H-DSKLEFIASKLA-OH) identified by Yin and coworkers that undergoes modification by PPTases, thereby serving as an ACP surrogate [29]. This choice was strengthened by the fact that solid phase peptide synthesis (SPPS) allows access to large quantities of uniformly labeled material, a crucial requirement for FRET applications, and avoids the potential for batch-to-batch variability. In selecting the placement of the label, we noted that YbbR was isolated as a collection of N-terminal extensions to the consensus, suggesting a site for modification that would not abrogate activity. As such, we chose to attach FITC to the YbbR consensus via a 6-aminocaproic acid spacer unit to sufficiently distance the molecule from the central motif (Fig. 3A) and impart a number of freely rotatable bonds, thereby ensuring a random spatial orientation on FRET pair assembly (*vide infra*).

In selecting complementary probes containing modest spectral overlap with FITC for mCoA **6** production, we sought maleimide-bearing compounds that were amenable to organic extraction after reaction with CoA (Fig. 3B) because this would circumvent HPLC purification, a characteristic that would make the procedure easily scaleable for a high-screening volume application. With this in mind, DACM **9** and TAMRA **10** were chosen and used to prepare DACM–mCoA **11** and TAMRA–mCoA **12** (Fig. 3B) to be evaluated as a FRET donor (Fig. 4A) and FRET acceptor (Fig. 4E), respectively.

HPLC analysis of the labeled substrates

The labeled substrates were evaluated by HPLC to probe the effects that modification of the substrates would have on the kinetic parameters displayed by the enzymes. Evaluation of FITC–YbbR **8** with AcpS and Sfp, with a saturating concentration of CoA **2**, returned K_m values of 86 and 101 μM, respectively, and k_{cat} values of 4.4 and 12.1 μM, respectively. These are in agreement with previously determined values for the unmodified substrate (K_m values of 200 and 123 μM for AcpS and Sfp, respectively) [29,30]. In addition, the kinetic parameters for TAMRA–mCoA **12** were determined at a saturating concentration of FITC–YbbR **8** and gave K_m values of 22 and 6 μM for AcpS and Sfp, respectively, with k_{cat} values of 3.2 and 8.9, respectively. Again, these values were found to be in agreement with previously determined parameters [29,30] and demonstrate that the modifications made to the substrates were well tolerated by the enzymes.

Determination of Förster radius

To assess the viability of the donor and acceptor substrates chosen, we sought to determine the theoretical Förster's radius (R_0) of these pairs. This value, the distance where transfer efficiency is

Table 1
Summarized assay protocol.

Step	Parameter	Value	Description
1	Compound library	2.5 μl	Transfer to Costar 3694 black 96-well plate; rows G and H = DMSO for control
2	Enzyme solution	37.5 μl	**1.33× solution**: 1.33 mg/ml BSA, 66.6 mM Na–Hepes, pH 7.6, 13.3 mM $MgCl_2$
3	Time	15 min	Room temperature incubation
4	Substrate reagent	10 μl	**5× solution**: 25 μM FITC–YbbR **8**, 50 μM TAMRA–mCoA **12** in 10 mM sodium phosphate
5	Detection	Ex 485, Em 535 nm	PerkinElmer HTS 7000 Plus, kinetic read, once every 2 min for 15 cycles

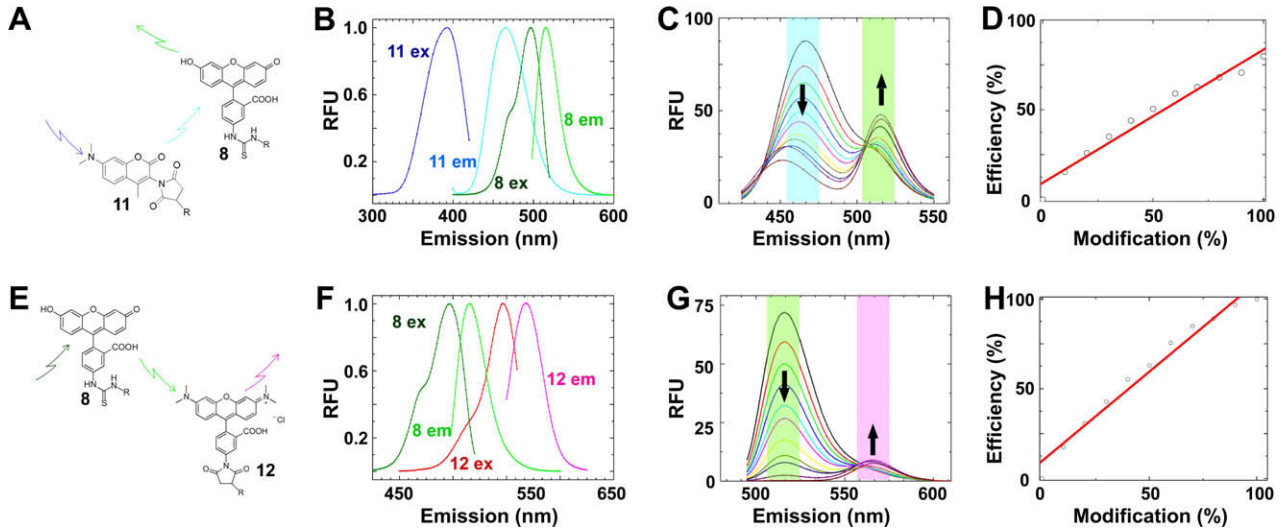

Fig. 4. Probe selection and photophysical evaluation of the *crypto*-YbbR peptides. DACM–mCoA **11** and TAMRA–mCoA **12** probes were evaluated for their FRET characteristics with FITC–YbbR **8**. (A) DACM–mCoA **11** acts as a FRET donor to FITC–YbbR **8**. (B) Excitation and emission spectra of probes **11** and **8** were recorded and normalized to determine the spectral overlap of **11** emission with **8** excitation to calculate an overlap integral $J(\lambda)$ (Eq. (3)) and a theoretical Förster's radius R_0 (Eq. (2)) of this system. Summation of the normalized data gave a $J(\lambda)$ of 1.60×10^{-13} cm^4 and an R_0 of 38 Å. (C) FRET characterization of the *crypto*-DACM–FITC–YbbR peptide. Equimolar solutions of **11** and **8** were prepared with varying degrees of modification to the *crypto*-DACM–FITC–YbbR **7**, and their fluorescent spectra were recorded with excitation at 403 nm. The spectra are overlaid and increase in 10% increments of modification from 0% to 100%, starting from the maximum emission observed at 462 nm to the minimum at this wavelength. (D) Eq. (5) was fitted to emission data from (C) and gave an efficiency of transfer value of 0.82. (E) FITC–YbbR **8** acts as a FRET donor to TAMRA–mCoA **12**. (F) Excitation and emission spectra of probes **8** and **12** were recorded and normalized to determine the spectral overlap of **8** emission with **12** excitation to calculate an overlap integral $J(\lambda)$ (Eq. (3)) and a theoretical Förster's radius R_0 (Eq. (2)) of this system. Summation of the normalized data gave a $J(\lambda)$ of 3.01×10^{-13} cm^4 and an R_0 of 56 Å. (G) FRET characterization of the *crypto*-TAMRA–YbbR peptide. Equimolar solutions of **8** and **12** were prepared with varying degrees of modification to the *crypto*-TAMRA–YbbR **7**, and their fluorescent spectra were recorded with excitation at 475 nm. The spectra are overlaid and increase in 10% increments of modification from 0% to 100%, starting from the maximum emission observed at 513 nm to the spectrum with the minimum value at this wavelength. (H) Eq. (5) was fitted to emission data at 513 nm from (G) and gave an efficiency of transfer value of 0.99.

50%, is related to donor quantum yield Φ_D, the relative orientation of donor and acceptor transition dipoles κ, and $J(\lambda)$, the overlap integral of the donor emission F_D and the absorption of the acceptor ε_A [31]:

$$R_0^6 = \frac{\Phi_D \kappa^2 9000(\ln 10)}{128\pi^5 N_A \eta^4} J(\lambda). \quad (1)$$

For κ, a value of 2/3 is assumed and corresponds to a random orientation of the two fluorophores in space given that they will be linked by numerous freely rotatable bonds. η, the index of refraction of the medium, is assumed to be 1.44 for biological samples [31], and N_A, Avogadro's number, is a constant, leaving R_0 to be determined by Φ_D and $J(\lambda)$. Quantum yields for these fluorophores were determined previously [32]. $J(\lambda)$ is expressed as

$$J(\lambda) = \int F_D(\lambda)\varepsilon_A(\lambda)\lambda^4 \delta\lambda. \quad (2)$$

Simple equations cannot be written for $F_D(\lambda)$ and $\varepsilon_A(\lambda)$; thus, $J(\lambda)$ is calculated as a summation [33]:

$$J(\lambda) \simeq \sum_{i=1}^{i=n} J_i = \sum_{i=1}^{i=n} F_D(\bar{\lambda}_i)\varepsilon_A(\bar{\lambda}_i)\bar{\lambda}_i^4 \Delta\lambda. \quad (3)$$

Absorption and emission spectra were recorded for the three conjugated substrates **8**, **11**, and **12** (Fig. 4B and F), and summation of the values at each wavelength according to Eq. (3) and use of these $J(\lambda)$ values in Eq. (1) gave Förster's radii of 38 and 56 Å for the DACM–FITC (Fig. 4A) and TAMRA–FITC pairs (Fig. 4E), respectively.

Photophysical evaluation of the phosphopantetheinylated peptide and efficiency of transfer determination

With the theoretical Förster's radii, we mathematically calculated the maximum distance that two fluorophores could achieve in the *crypto*-FITC–YbbR product (exemplified as **7** in Fig. 2) by summation of average bond lengths and determined this to be 42 Å (radius [r] of 21 Å) if a rigid linear extension were to occur. This suggests a high theoretical FRET efficiency, E, which is strictly related to the radius separating the two fluorophores, r, by

$$E = \frac{R_0^6}{R_0^6 + r^6}, \quad (4)$$

with a rapid decay in E when r exceeds R_0. Using the R_0 values determined from Eq. (1) and our calculated r of 21 Å, Eq. (4) gives theoretical E values of 97% and 99% for the DACM–FITC and TAMRA–FITC pairs, respectively. However, r exists as a distribution due to the number of freely rotatable bonds; thus, transfer efficiency must be determined experimentally by measurement of donor fluorescence in the absence (F_D) or presence (F_{DA}) of acceptor and fitting of Eq. (5) to the experimental data:

$$E = 1 - \frac{F_{DA}}{F_D}. \quad (5)$$

Reactions were set up with mCoA analogues **11** and **12**, Sfp, and FITC–YbbR **8** and were followed to completion by HPLC. The corresponding *crypto*-FITC–YbbR **7** peptides were then isolated by semi-preparative HPLC. These products were used to prepare equimolar mixtures of the probes with varying degrees of modification. Fluorescent emission spectra of these mixtures were recorded (Fig. 4C and G). Analysis of these data (Fig. 4D and H) by Eq. (5) yields efficiency of transfers of 0.82 and 0.99 for the DACM–FITC (Fig. 4A) and TAMRA–FITC (Fig. 4E) pairs, respectively.

Mode of observation

Data in Fig. 4C and G are also informative with regard to the mode of monitoring for this biochemical system. FRET pairs offer

flexibility in that their assembly can be detected either by the quench of the donor emission (down arrows) or by the sensitization of acceptor fluorescence at shorter excitation wavelengths (up arrows). Evaluation of data for both systems shows a greater response for the quenching mode, with fivefold and 10-fold reductions in donor fluorescence on conversion to *crypto*-FITC–YbbR **7** for the DACM–FITC and TAMRA–FITC pairs, respectively. Evaluation of acceptor sensitized emission at shorter excitation wavelengths showed an increase of twofold for complete conversion, indicating that the system would give a greater signal-to-background ratio by monitoring the quench of donor fluorescence. Therefore, this screen would function optimally as a substrate consumption assay.

Of these two FRET systems, TAMRA–mCoA probe **12** possessed better FRET characteristics (i.e., full attenuation of donor fluorescence on complete conversion) and was chosen to be carried forward for screen implementation.

Determination of screen conditions

We arrived at initial assay conditions based on the requirement that the end point would need complete attenuation of donor fluorescence; requiring TAMRA–mCoA **12** to be present in excess of FITC–YbbR **8**. With this in mind, we probed the linearity of detector response with respect to FITC–YbbR **8** concentration. This was done to identify the maximum concentration that could be obtained before direct correlations between relative fluorescence units (RFU) and substrate concentration became obscured by an inner filter effect, a phenomenon where all incident light irradiated on the sample is absorbed and does not sufficiently transition all target molecules to the excited state. With our plate reader (PerkinElmer HTS7000), we found delineation to occur at concentrations exceeding 10 μM; thus, we chose to hold FITC–YbbR **8** at a concentration of 5 μM.

We then sought to determine the effects of increasing the concentration of TAMRA–mCoA **12** on FITC–YbbR **8** signal. The purpose of this analysis was to find an acceptably high concentration of TAMRA–mCoA **12** that did not impart an effect on FITC–YbbR **8** emission as it displays some absorption at the FITC–YbbR **8** excitation wavelengths. We found the signal to be maintained at concentrations up to 12.5 μM, and we arrived at the final concentration in the screen for TAMRA–mCoA **12** to be 10 μM.

Assay optimization: requirement of BSA for enzyme stability

The screen was first developed by initiating reactions in 96-well plates with varied enzyme concentrations. These experiments were monitored continuously using standard fluorescein optics, and analysis of the progress curves revealed that the reaction rate did not follow linearly with respect to enzyme concentration. This was identified to be a complication with time-dependent inactivation of the enzyme using Selwyn's method [34] (data not shown). A number of reaction additives, including buffer and salt composition, ionic strength, and detergents, were screened in an attempt to stabilize the enzyme, and we found that inclusion of BSA at a concentration of 1 mg/ml (15 μM) stabilized the enzyme and eliminated this complication.

With this modification, stable reaction progress plots (Fig. 5A and C) that displayed a linear relationship between rate and enzyme concentration (Fig. 5B and D) were observed. From these data, we determined optimum enzyme concentrations to be 50 and 12.5 nM for AcpS and Sfp, respectively, based on obtaining a complete progress curve terminating in approximately 30% substrate consumption over a 30-min time interval (*vide infra*). It is noteworthy that although inclusion of BSA may traditionally be considered as unattractive in a screening campaign, this carrier provides an excellent source of amine and thiol moieties and may serve to repress inhibition of the enzyme by nonspecific electrophilic species present in diverse compound libraries.

DMSO tolerance

Because most compound libraries are stocked as solutions in DMSO, we sought to evaluate the tolerance of the screen to this organic solvent. Inclusion of any organic solvent in the reaction caused an immediate 10% increase in RFU signal from the substrate

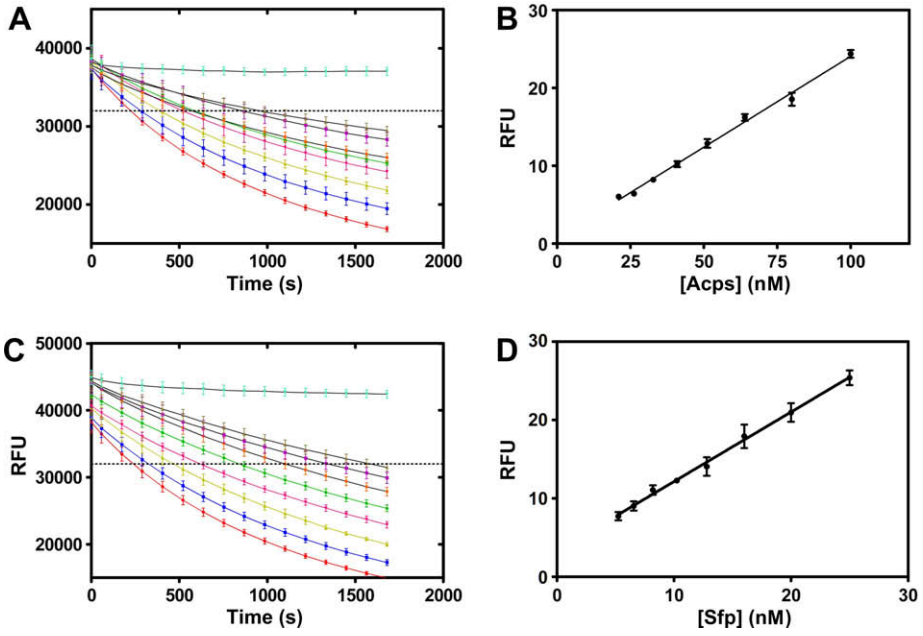

Fig. 5. Reaction progress and enzyme titration. (A) Reaction progress plots for eight concentrations of AcpS. Rates were determined for the experiments when they intersect the dashed threshold at 32,000 RFU. (B) Reaction rates for the progress curves in (A) are plotted against AcpS concentration and demonstrate a linear response. (C) Reaction progress curves for eight concentrations of Sfp. Rates were determined for the experiments when they intersect the dashed threshold at 32,000 RFU. (D) Reaction rates for the progress curves in (C) are plotted against Sfp concentration and demonstrate a linear response.

mixture but did not deteriorate the observed rate until reaching a concentration greater than 10% total volume (data not shown). For our routine screening conditions, we maintained a final DMSO concentration of 5% (v/v).

Progress curve analysis and signal statistics

With final assay conditions in hand, a screening protocol was developed and is presented in Table 1. Following this protocol, we recorded progress curves and analyzed these data statistically to determine the appropriate time for analysis. Because known inhibitors of PPTases are not commercially available, an enzyme-free reaction was used as the fully inhibited (negative) control. Analysis of these data (presented in Fig. 6A and B) demonstrated that the assay performance relied heavily on the amount of substrate consumption that was allowed to occur, with the parameter values becoming better with further consumption (Table 2). However, excessive substrate consumption can lead to erroneous determination of inhibition characteristics [35], and a progression of approximately 20% (Table 2, boxed values) was chosen as a balance of conditions where a minimum of substrate was consumed and assay statistics reached acceptable values, including Z' values of 0.7 and signal-to-noise values of 20 (Table 2).

Subsequently, this experiment was repeated on three separate days to assess the robustness of the method, and the data are presented in Table 3. The Z' factor [36] is often used to evaluate the suitability of a screening method for high-throughput implementation, with values greater than 0.5 being considered as satisfactory.

Table 3
Day-to-day variability.

Statistical value	AcpS	Sfp
Z'	0.75 ± 0.02	0.72 ± 0.01
Signal/Noise	23.1 ± 2.1	19.9 ± 1.2
Signal/Background	10.8 ± 0.3	11.7 ± 1.5
Signal window	17.3 ± 2.0	14.3 ± 1.1

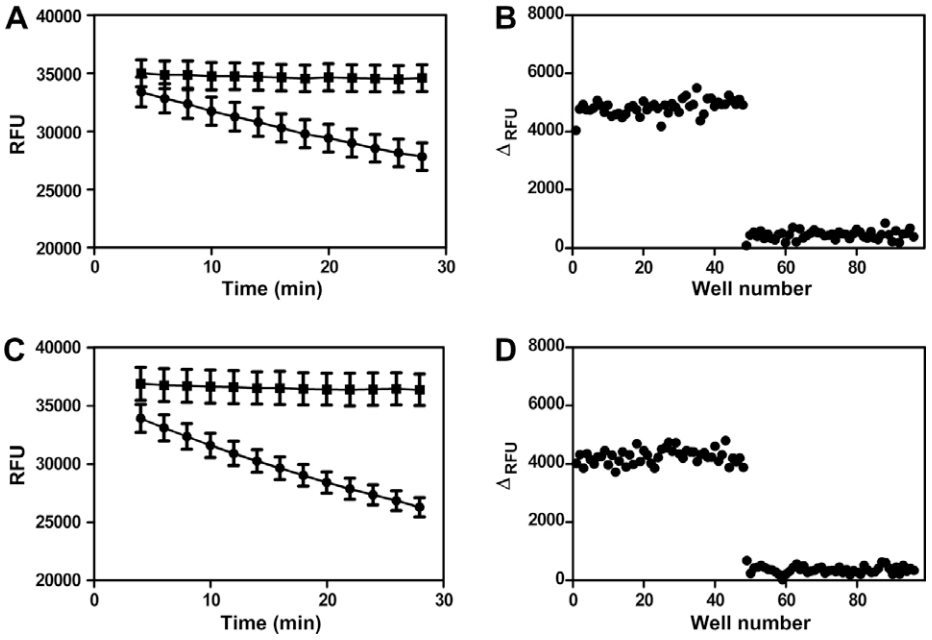

Fig. 6. Determination of analysis time point and Z'. (A) Progress curve for a 96-well plate containing 48 reactions in the presence (●) and absence (■) of 50 nM AcpS. The data for each time point were analyzed statistically and are presented in Table 2. The 24-min time point was selected for routine analysis because it gave acceptable assay statistics during the linear range of the screen. (B) The change in RFU for the 24-min time point (Table 2, boxed data) is plotted against well number. The Z' value for these data is 0.72. (C) Progress curve for a 96-well plate containing 48 reactions in the presence (●) and absence (■) of 12.5 nM Sfp. The data for each time point were analyzed statistically and are presented in Table 2. The 16-min time point was selected for routine analysis because it gave acceptable assay statistics during the linear range of the screen. (D) The change in RFU for the 16-min time point (Table 2, boxed data) is plotted against well number. The Z' value for these data is 0.71.

Table 2
Statistical analysis of 50-nM AcpS and 12.5-nM Sfp progress curves.

	Time (minutes)											
	6	8	10	12	14	16	18	20	22	24	26	28
AcpS												
Z'	−0.92	0.02	0.35	0.47	0.59	0.59	0.68	0.68	0.72	0.71	0.74	0.74
Signal/Noise	3.1	6.1	9.2	11.2	14.6	14.6	18.3	18.5	20.5	20.2	21.8	21.9
Signal/Background	4.0	8.2	6.4	8.4	8.6	8.3	8.1	11.4	10.7	10.8	10.7	13.3
Signal window	−2.9	0.1	3.2	5.2	8.7	8.7	12.5	12.6	14.9	14.4	16.0	16.2
Sfp												
Z'	−0.11	0.33	0.51	0.62	0.64	0.70	0.70	0.73	0.76	0.76	0.77	0.78
Signal/Noise	5.4	8.9	12.2	15.4	15.5	19.2	19.4	20.8	23.5	23.4	24.5	25.5
Signal/Background	7.0	8.8	9.3	10.1	10.0	11.6	10.8	11.4	11.9	14.0	15.9	14.6
Signal window	−0.6	2.9	6.2	9.6	9.9	13.5	13.7	15.2	17.8	17.8	19.0	19.9

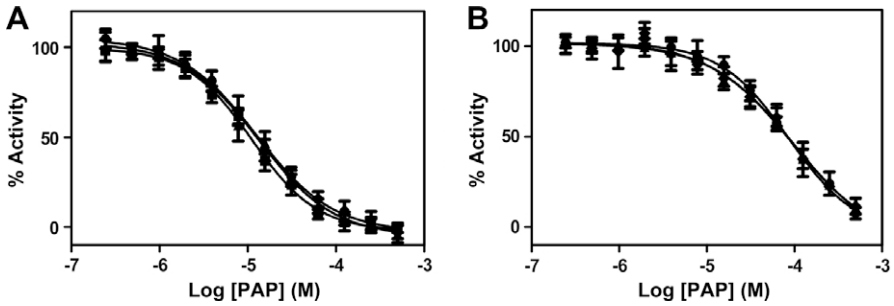

Fig. 7. Reproducibility of IC_{50} values for PAP. (A) Sfp was screened against 12 concentrations of PAP ranging from 244 nM to 500 μM on three separate days. The data were fit with the four-parameter dose–response curve using GraphPad Prism software and returned IC_{50} values of 13, 11, and 13 μM. (B) Replication of the same experiment as in (A) except using the AcpS enzyme. These curves returned IC_{50} values of 86, 98, and 94 μM.

The assay performed well and gave Z' values of 0.72 ± 0.01 and 0.75 ± 0.02 for Sfp and AcpS, respectively.

Screen validation for inhibitor identification

To demonstrate the ability of this screen to identify inhibitors of PPTases, we evaluated the effects of product inhibition by PAP **3** (Fig. 1), the nucleotide product released by the enzyme, used by McAllister and coworkers in their studies of the reaction mechanism of AcpS [13]. PAP was serial diluted (twofold) from a top concentration of 10 mM in DMSO and stocked in polypropylene plates and was evaluated in the assay with both enzymes on three separate days (Fig. 7), again to demonstrate reproducibility of the screen. The method proved to yield consistent inhibition curves, with IC_{50} values of 12.3 ± 1.1 and 92 ± 6 μM for Sfp and AcpS, respectively, and Hill coefficients for these analyses of −1.06 ± 0.09 and −0.98 ± 0.11 for Sfp and AcpS, respectively. Taken together, these data support the suitability of this method to determine inhibitory characteristics of compounds for these PPTase enzymes.

Conclusions

We have developed a homogeneous screen for PPTase that requires a minimum number of liquid handling steps and meets the criteria set forth by the National Institutes of Health Chemical Genomics Center as acceptable for automation [37]. Importantly, this method uses simple reagents that can be prepared through traditional techniques [24,38] and are pure chemical entities that do not require interbatch standardization, a luxury not afforded by complex biochemical reagents. It is anticipated that this method can be used to evaluate the cross-reactivity of currently known AcpS inhibitors and to identify new inhibitor architectures for Sfp and AcpS, and this work is currently in progress.

Acknowledgments

This work was funded by National Institutes of Health (NIH) R01GM075797 and 1R03MH083266. We thank Christopher T. Walsh (Harvard Medical School) for plasmids containing the Sfp and AcpS expression systems, Elizabeth A. Komives for guidance and assistance with peptide synthesis, and Adam Yasgar and Anton Simeonov (NIH Chemical Genomics Center) for helpful discussions.

References

[1] R.H. Lambalot, A.M. Gehring, R.S. Flugel, P. Zuber, M. LaCelle, M.A. Marahiel, R. Reid, C. Khosla, C.T. Walsh, A new enzyme superfamily: the phosphopantetheinyl transferases, Chem. Biol. 3 (1996) 923–936.

[2] L.E. Quadri, P.H. Weinreb, M. Lei, M.M. Nakano, P. Zuber, C.T. Walsh, Characterization of Sfp, a *Bacillus subtilis* phosphopantetheinyl transferase for peptidyl carrier protein domains in peptide synthetases, Biochemistry 37 (1998) 1585–1595.

[3] N. Barekzi, S. Joshi, S. Irwin, T. Ontl, H.P. Schweizer, Genetic characterization of pcpS, encoding the multifunctional phosphopantetheinyl transferase of *Pseudomonas aeruginosa*, Microbiology 150 (2004) 795–803.

[4] R. Finking, J. Solsbacher, D. Konz, M. Schobert, A. Schafer, D. Jahn, M.A. Marahiel, Characterization of a new type of phosphopantetheinyl transferase for fatty acid and siderophore synthesis in *Pseudomonas aeruginosa*, J. Biol. Chem. 277 (2002) 50293–50302.

[5] R.H. Lambalot, C.T. Walsh, Cloning, overproduction, and characterization of the *Escherichia coli holo*-acyl carrier protein synthase, J. Biol. Chem. 270 (1995) 24658–24661.

[6] K.D. Parris, L. Lin, A. Tam, R. Mathew, J. Hixon, M. Stahl, C.C. Fritz, J. Seehra, W.S. Somers, Crystal structures of substrate binding to *Bacillus subtilis holo*-(acyl carrier protein) synthase reveal a novel trimeric arrangement of molecules resulting in three active sites, Struct. Fold. Des. 8 (2000) 883–895.

[7] K. Reuter, M.R. Mofid, M.A. Marahiel, R. Ficner, Crystal structure of the surfactin synthetase-activating enzyme Sfp: a prototype of the 4′-phosphopantetheinyl transferase superfamily, EMBO J. 18 (1999) 6823–6831.

[8] H.M. Lam, E. Tancula, W.B. Dempsey, M.E. Winkler, Suppression of insertions in the complex Pdxj operon of *Escherichia coli* K–12 by ion and other mutations, J. Bacteriol. 174 (1992) 1554–1567.

[9] H.E. Takiff, T. Baker, T. Copeland, S.M. Chen, D.L. Court, Locating essential *Escherichia coli* genes by using mini-Tn10 transposons: the Pdxj operon, J. Bacteriol. 174 (1992) 1544–1553.

[10] M. Chu, R. Mierzwa, L. Xu, S.W. Yang, L. He, M. Patel, J. Stafford, D. Macinga, T. Black, T.M. Chan, V. Gullo, Structure elucidation of Sch 538415, a novel acyl carrier protein synthase inhibitor from a microorganism, Bioorg. Med. Chem. Lett. 13 (2003) 3827–3829.

[11] A.M. Gilbert, M. Kirisits, P. Toy, D.S. Nunn, A. Failli, E.G. Dushin, E. Novikova, P.J. Petersen, D. Joseph-McCarthy, I. McFadyen, C.C. Fritz, Anthranilate 4H-oxazol-5-ones: novel small molecule antibacterial acyl carrier protein synthase (AcpS) inhibitors, Bioorg. Med. Chem. Lett. 14 (2004) 37–41.

[12] D. Joseph-McCarthy, K. Parris, A. Huang, A. Failli, D. Quagliato, E.G. Dushin, E. Novikova, E. Severina, M. Tuckman, P.J. Petersen, C. Dean, C.C. Fritz, T. Meshulam, M. DeCenzo, L. Dick, I.J. McFadyen, W.S. Somers, F. Lovering, A.M. Gilbert, Use of structure-based drug design approaches to obtain novel anthranilic acid acyl carrier protein synthase inhibitors, J. Med. Chem. 48 (2005) 7960–7969.

[13] K.A. McAllister, R.B. Peery, T.I. Meier, A.S. Fischl, G. Zhao, Biochemical and molecular analyses of the *Streptococcus pneumoniae* acyl carrier protein synthase, an enzyme essential for fatty acid biosynthesis, J. Biol. Chem. 275 (2000) 30864–30872.

[14] D.J. Payne, M.N. Gwynn, D.J. Holmes, D.L. Pompliano, Drugs for bad bugs: confronting the challenges of antibacterial discovery, Nat. Rev. Drug Discov. 6 (2007) 29–40.

[15] J. Neres, N.P. Labello, R.V. Somu, H.I. Boshoff, D.J. Wilson, J. Vannada, L. Chen, C.E. Barry, E.M. Bennett, C.C. Aldrich, Inhibition of siderophore biosynthesis in *Mycobacterium tuberculosis* with nucleoside bisubstrate analogues: Structure–activity relationships of the nucleobase domain of 5′-*O*-[*N*-(salicyl)sulfamoyl]adenosine, J. Med. Chem. 51 (2008) 5349–5370.

[16] K.L. Stirrett, J.A. Ferreras, V. Jayaprakash, B.N. Sinha, T. Ren, L.E.N. Quadri, Small molecules with structural similarities to siderophores as novel antimicrobials against *Mycobacterium tuberculosis* and *Yersinia pestis*, Bioorg. Med. Chem. Lett. 18 (2008) 2662–2668.

[17] J.A. Ferreras, K.L. Stirrett, X.Q. Lu, J.S. Ryu, C.E. Soll, D.S. Tan, L.E.N. Quadri, Mycobacterial phenolic glycolipid virulence factor biosynthesis: Mechanism and small-molecule inhibition of polyketide chain initiation, Chem. Biol. 15 (2008) 51–61.

[18] J.S. Cisar, J.A. Ferreras, R.K. Soni, L.E.N. Quadri, D.S. Tan, Exploiting ligand conformation in selective inhibition of non-ribosomal peptide synthetase

amino acid adenylation with designed macrocyclic small molecules, J. Am. Chem. Soc. 129 (2007) 7752.
[19] J.L. Meier, T. Barrows-Yano, T.L. Foley, C.L. Wike, M.D. Burkart, The unusual macrocycle forming thioesterase of mycolactone, Mol. BioSyst. 4 (2008) 663–671.
[20] R.H. Lambalot, C.T. Walsh, *Holo*-[acyl-carrier-protein] synthase of *Escherichia coli*, in: J. Abelson, D. McCormick, M. Simon, J. Suttie, C. Wagner (Eds.), Methods in Enzymology: Vitamins and Coenzymes, Part I, vol. 279, Academic Press, San Diego, 1997, pp. 254–262.
[21] K.J. Glover, P.M. Martini, R.R. Vold, E.A. Komives, Preparation of insoluble transmembrane peptides: Glycophorin-A, prion (110–137), and FGFR (368–397), Anal. Biochem. 272 (1999) 270–274.
[22] J. Inglese, R.L. Johnson, A. Simeonov, M.H. Xia, W. Zheng, C.P. Austin, D.S. Auld, High-throughput screening assays for the identification of chemical probes, Nat. Chem. Biol. 3 (2007) 466–479.
[23] E.F. Pettersen, T.D. Goddard, C.C. Huang, G.S. Couch, D.M. Greenblatt, E.C. Meng, T.E. Ferrin, UCSF chimera: a visualization system for exploratory research and analysis, J. Comput. Chem. 25 (2004) 1605–1612.
[24] J.J. La Clair, T.L. Foley, T.R. Schegg, C.M. Regan, M.D. Burkart, Manipulation of carrier proteins in antibiotic biosynthesis, Chem. Biol. 11 (2004) 195–201.
[25] J.A. Haas, M.A. Frederick, B.G. Fox, Chemical and posttranslational modification of *Escherichia coli* acyl carrier protein for preparation of dansyl–acyl carrier proteins, Protein Expr. Purif. 20 (2000) 274–284.
[26] P.G. Blommel, B.G. Fox, Fluorescence anisotropy assay for proteolysis of specifically labeled fusion proteins, Anal. Biochem. 336 (2005) 75–86.
[27] N.S. Joshi, L.R. Whitaker, M.B. Francis, A three-component Mannich-type reaction for selective tyrosine bioconjugation, J. Am. Chem. Soc. 126 (2004) 15942–15943.
[28] T.L. Schlick, Z.B. Ding, E.W. Kovacs, M.B. Francis, Dual-surface modification of the tobacco mosaic virus, J. Am. Chem. Soc. 127 (2005) 3718–3723.
[29] J. Yin, P.D. Straight, S.M. McLoughlin, Z. Zhou, A.J. Lin, D.E. Golan, N.L. Kelleher, R. Kolter, C.T. Walsh, Genetically encoded short peptide tag for versatile protein labeling by Sfp phosphopantetheinyl transferase, Proc. Natl. Acad. Sci. USA 102 (2005) 15815–15820.
[30] Z. Zhou, P. Cironi, A.J. Lin, Y.Q. Xu, S. Hrvatin, D.E. Golan, P.A. Silver, C.T. Walsh, J. Yin, Genetically encoded short peptide tags for orthogonal protein labeling by sfp and AcpS phosphopantetheinyl transferases, ACS Chem. Biol. 2 (2007) 337–346.
[31] J.R. Lakowicz, Principles of Fluorescence Spectroscopy, Kluwer Academic/Plenum, New York, 1999.
[32] M. Machida, N. Ushijima, M.I. Machida, Y. Kanaoka, *N*-(7-Dimethylamino-4-methyl-coumarin-yl) maleimides (DACM): novel fluorescent thiol reagents, Chem. Pharm. Bull. 23 (1975) 1385–1386.
[33] I.D. Campbell, R.A. Dwek, R.A. Dwek, Biological Spectroscopy, Benjamin Cummings, Menlo Park, CA, 1984.
[34] M.J. Selwyn, A simple test for inactivation of an enzyme during assay, Biochim. Biophys. Acta 105 (1965) 193–194.
[35] G. Wu, Y. Yuan, C.N. Hodge, Determining appropriate substrate conversion for enzymatic assays in high-throughput screening, J. Biomol. Screen. 8 (2003) 694–700.
[36] J.H. Zhang, T.D.Y. Chung, K.R. Oldenburg, A simple statistical parameter for use in evaluation and validation of high throughput screening assays, J. Biomol. Screen. 4 (1999) 67–73.
[37] NIH Chemical Genomics Center, NCGC High Throughput Screening Assay Guidance Criteria, 2009. Available from: <http://www.ncgc.nih.gov/guidance/HTS_Assay_Guidance_Criteria.html>.
[38] D.A. Wellings, E. Atherton, Standard Fmoc protocols, Methods Enzymol. 289 (1997) 44–67.